Impulse Response Model for Switched Inductor Converters

Ryan J. Billing

Schweitzer Engineering Laboratories

ryan_billing@selinc.com

Joseph Amodemo

Schweitzer Engineering Laboratories

joseph_amodemo@selinc.com

Abstract—**The transfer function of a switched inductor converter is developed based upon analysis of the impulse response of the perturbed system. A new equivalent circuit model is introduced in which the inductor charging and discharging cycle currents are expressed (each) as a behavioral current source generating a sequence of current pulses matching the inductor currents that result from a perturbed system. The proposed approach deconstructs the switched inductor system impulse response into a system of cascaded discrete-time filters, then reconstructs the continuous-time output which is realized within the current source models.**

The analysis technique is demonstrated by considering the control-to-output transfer function of a converter operating in current programmed mode (CPM). The CPM converter is expressed by a cascade combination of an IIR filter expressing control-to-valley current, which is then chained into a filter reversing the Zero-Order-Hold (ZOH) assumption used to work out control-to-valley transfer function. Finally, two sets of FIR filters are used to express valley-to-average and average-to-pulse for the charging and discharging cycle inductor current.

The control-to-output transfer function is shown to match what is found in conventional literature, however, the final average-to-pulse FIR filter is not found in averaged switch models. This final FIR stage reproduces the correct group delay, making the phase response accurate up to the Nyquist rate. The consequence of using the final stage in the model is shown by comparing simulation results from the new model, a conventional model and measured data from a fixed frequency flyback converter.

I. Introduction

Switched-mode power converters are the power electronics industry's practical implementation for what otherwise might be considered a purely theoretical DC transformer. High-frequency commutation of voltage across an inductor affords controlled storage and release of energy between power sources and loads. The primary benefits include accurate regulation, small physical size and minimal dissipative loss (high power density).

Implementation of a switched-mode converter is not without challenges. In addition to other difficulties outside the scope of this document, it is here brought to the forefront that controlling such a system is nontrivial: the control-loop dynamics are emphatically not Linear, Time-Invariant (LTI) systems.

The conventional approach used to express the transfer function for switched inductor converters considers the average behavior of the switch element as a continuous-time impedance. In this approach the system dynamic behavior is evaluated by modulating the switch's average impedance as a function of duty cycle. The modulator gain of the Averaged Switch Model may be applied as a nonlinear impedance for use in numerical simulations, or as a small-signal linear system for analytical characterization.

The most notable cleverness in the conventional approach is the ability to treat the switch element as a three-terminal device that is characterized using only terminal voltages and currents. This switch model may be placed in any configuration to represent a large subset of switched-mode converters. Generalization of the switch element allows for development of a unified model capturing dynamic behavior of switched-mode converters over a broader class of converter topologies. With the switch modeled as a nonlinear impedance element, there is no need to re-evaluate fundamental assumptions about averaging of the switch's dynamic behavior when using the model to evaluate most converter topologies.

One behavior missing from an averaged system is a model for the inherent sampling sub-system. Specifically, the system intakes (samples) and expels a discrete quantity of energy within each switching cycle. A model neglecting the sampling effect loses visibility into a part of the dynamic behavior prominent above $\frac{1}{4}F_{SW}$ and has material impact on evaluation of the system's gain margin while also neglecting artifacts of the control system (such as subharmonic oscillation in a peak current-mode controller).

The sampling effect was addressed in a further development to the averaged converter behavior presented by Tan, Middlebrook in [ref]. This document introduces a sampler and approximates its effect in the frequency domain to account for it in the averaged model. The sampling effect as introduced by Tan, Middlebrook when coupled with the averaged switch model completes a unified model with improved accuracy in the magnitude response, having negligible error up to the converter Nyquist rate.

As demonstrated by Jian Li in [ref], the Tan/Middlebrook unified model still fails to predict the high frequency phase response under all conditions. A further shortcoming identified by Li of the traditional (and enhanced) averaging models is scalability, e.g., accuracy further diminishes when used to approximate variable frequency controllers.

II. An Alternative Approach

This document revisits the problem of characterizing dynamic behavior in switched mode converters with the aim of

TOPOLOGY	SWITCHED-MODE MODEL	BEHAVIORAL CURRENT SOURCE MODEL
BUCK		
BOOST		
BUCK/ BOOST		
ISOLATED FLYBACK		
ISOLATED FORWARD (ACTIVE CLAMP)		

Fig. 1: Review of switched-mode power converter topologies and equivalent circuit model used for developing the impulse response derived transfer functions.

exposing a closer link between transfer function elements in the waveform geometry. The defining feature of this approach is consideration for the link between a system's impulse response and frequency response. Like other approaches, the non-LTI nature of the system is simplified by using small-signal analysis techniques to linearize the response at a pre-determined operating point. In this case, all system variables are held constant while a single impulse is applied to one

and the system response would be derived for each input. In this document the scope is limited to derivation of control-to-output transfer function, focusing on the technique rather than producing complete models.

The equivalent circuit model is prepared by combining the inductor and switch together as a pair of behavioral current sources as shown in Fig. 1. The currents i_{cg} and i_{dg} correspond to charging and discharging inductor currents where control-to-current transfer functions are expressed as a set of cascaded filters. The geometry of switched current waveforms serve as a specification for the time-domain impulse responses for continuous time filters in this system's transfer function.

Several common switched inductor topologies are identified in Fig. 1 to better illustrate how this alternative model is substituted for the switch and inductor in the greater context of a switched-mode converter circuit. Note the left-hand models of Fig. 1 follow the 3-terminal switch construct as presented by Erickson/Maksimovic in [ref]. For these circuits the center position (no-connect) of the switch is considered a legal state so the switch may open when reverse-biased to allow modeling diode behavior.

III. CURRENT PROGRAMMED MODE CONTROL SYSTEM

At this point the proposed approach has been prepared in a generalized form. The next step is to derive expressions for i_{cg} and i_{dg} as a function of known quantities. To this end, a specific control scheme must be considered. Peak current programmed mode is chosen as an example because of the widespread availability of reference designs and switched-mode converter controller IC's using this control implementation.

Peak Current Programmed Mode Control is a technique used for controlling inductor currents in a switched-mode converter on a cycle-by-cycle decision-making interval. The control signal sets a threshold to limit inductor peak intake currents during the charging portion of the switching cycle. When the inductor current crosses this threshold, a latch is reset to signal shut-down of the primary switch device. A compensating ramp is often added to the controller current sense signal to induce pre-mature tripping of the comparator – a technique used to stabilize the peak current control loop.

IV. EXTRACTION OF THE IMPULSE RESPONSE

The diagram in Fig. 2 steps through the analytical process used to understand some key features in the inductor waveform that can be used to express the system impulse response.

The most helpful observations come to mind when the converter is considered to be a discrete time system at its core. Specifically, there is a discrete amount of energy intake during the charging cycle and a discrete amount of energy delivered to the output during the discharging cycle. When the converter is operating in Continuous Conduction Mode (CCM) there is a discrete amount of energy remaining in the inductor at the end of each cycle.

The variable most easy to express at the start of each switching interval is the valley current. Geometrically it is easy
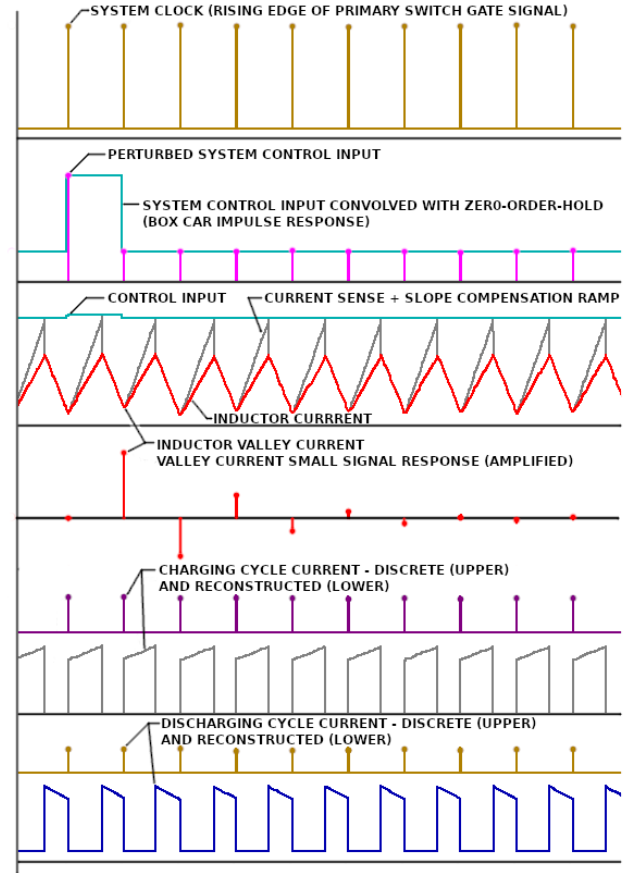

Fig. 2: Extraction of the impulse response is done by evaluating system behavior resulting from the application of a pulse. The impulse response is obtained by deconvolving the pulse pulse response and the pulse.

to see the previous valley current is linearly related to the next valley current if all system variables are held constant during the switching cycle. By superposition, all variables may be held constant and a perturbation may be applied exactly at the moment the peak current is about to exceed the threshold, but expressing this mathematically is difficult and physically unintuitive.

A way around this problem of injecting the impulse at exactly the correct time is to conclude that the system inputs are band-limited to the Nyquist rate, or that we don't care that aliasing effects are neglected. Given the assumption of band-limited inputs, all these signals can be sampled synchronously to the rising edge of the primary switching signal and then convolved with a Zero-Order-Hold (ZOH) filter function to create a geometric problem that is trivial to solve. The box car function is reversible so the valley current filter output can be corrected by application of an inverse of the ZOH.

Another way of looking at this is to consider the switching converter's pulse response rather than the impulse response, and then extracting the impulse response by deconvolving the output function from the input pulse.

A. Derivation of IIR Filter Describing Valley Currents

The analytical system presented in Fig. 3 shows the peak current threshold being sampled synchronous to the valley currents and then held constant throughout the switching cycle. Charging and discharging slopes are sampled values held static throughout the sampling interval, and the compensating ramp is considered linear (constant). This system is geometrically characterized using values sampled at the rising edge of the primary gate drive signal (coincident with inductor valley currents). A noteworthy advantage of this approach is the input and output impedance and coupling can be expressed as a discrete-time system. The effect of ZOH function applies equally to all sampled values and is reversed with a single operation on the valley currents using the distributive property of convolution. It will be shown in the derivation of averaging and reconstruction stages that the pulse shape and per-cycle energy are geometrically anchored in the valley currents.
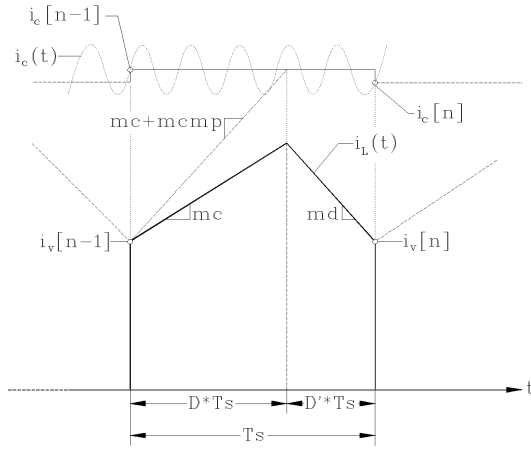

Fig. 3: Inductor waveforms with peak current mode control.

A formula relating one valley current to the next is the following,

$$i_v[n] = i_v[n-1] + m_c D T_{SW} - m_d D' T_{SW} \quad (1)$$

where,

$T_{SW} =$ Modulator switching (sampling) period
$D =$ Modulator duty cycle
$D' = (1 - D)$
$m_c =$ Slope of current during charge cycle (A/s)
$m_d =$ Slope of current during discharge cycle (A/s)
$i_v =$ Inductor valley current.

The duty cycle is re-expressed in the following terms,

$$D = \frac{i_c[n-1] - i_v[n-1]}{(m_c + m_{cmp})T_{SW}} \quad (2)$$

where,

$m_{cmp} =$ Slope compensation (A/s)
$i_c =$ Sampled peak current threshold.

Then expanding D and D' in (1), the following recurrence relation emerges,

$$i_v[n] = \alpha i_c[n-1] + (1-\alpha)i_v[n-1] - T_{SW}m_d \quad (3)$$

where,

$$\alpha = \frac{m_c + m_d}{m_c + m_{cmp}} \quad (4)$$

It is now apparent from (3) the peak current controller has the form of a discrete-time first order IIR filter. Note the IIR filter is an exact representation of the behavior that would be observed if all of its inputs were sampled and reconstructed using the ZOH reconstruction filter. The significance of this observation is the response to a single impulse is perfectly captured when the single impulse is first convolved with a ZOH response, the effect of which can be reversed easily in the frequency domain.

B. Z-transform of the Peak Current Controller

Given a difference equation for an LTI system (as assumed in (3)) the z-transform can be evaluated by inspection.

$$\mathcal{Z}\{i_v[n]\} = \alpha I_c(z)z^{-1} + (1-\alpha)I_v(z)z^{-1} - \mathcal{Z}\{T_{SW}m_d\} \quad (5)$$

The expression in (5) is easily rearranged into a canonical form transfer function if the Z-transform of the constant term is resolved.

$$\mathcal{Z}\{T_{SW}m_d\} = 0 \quad (6)$$

One way to dismiss the effect of the constant seen in (3) is by use of the unit step response, time shift and time reversal properties of the z-transform.

The necessary relationships are included to maintain coherence in the approach being presented.

TABLE I: Selected Z-transform Properties

Description	Time Domain	Z-tranform
Unit Step Response	$u[n] = \begin{cases} 0 & n < 0 \\ 1 & n \geq 0 \end{cases}$	$U(z) = \dfrac{1}{1 - z^{-1}}$
Time Reversal	$u[-n]$	$U(z^{-1}) = \dfrac{-z^{-1}}{1 - z^{-1}}$
Unit Delay	$u[n-1]$	$U(z)z^{-1} = \dfrac{z^{-1}}{1 - z^{-1}}$

The choice of relationships expressed in Table I plays on the following time-domain property.

$$u[n-1] + u[-n] = 1 \quad (7)$$

The expression in (7) is used to substitute unity in the constant expression, $T_{SW}m_d$,

$$\mathcal{Z}\{T_{SW}m_d\} = \mathcal{Z}\{T_{SW}m_d(u[n-1] + u[-n])\} \quad (8)$$

hence,

$$\mathcal{Z}\{T_{SW}m_d\} = T_{SW}m_d\left(\frac{z^{-1}}{1-z^{-1}} + \frac{-z^{-1}}{1-z^{-1}}\right) = 0 \quad (9)$$

Having reasonably dismissed the constant term, (5) is refactored to the following transfer function,

$$H_v(z) = \frac{I_v(z)}{I_c(z)} = \frac{\alpha z^{-1}}{1-(1-\alpha)z^{-1}} \quad (10)$$

C. Peak Current Controller Stability Analysis

The expression in (10) becomes unstable in cases when the system is defined outside of the Region of Convergence (ROC) or the denominator approaches zero. Using Euler's formula, the complex exponential term in the denominator expands to the following.

$$z^{-1} = e^{-j\omega T_{SW}} = \cos(\omega T_{SW}) - j\sin(\omega T_{SW}) \quad (11)$$

The condition for which it is possible for the denominator to become zero is at frequency $\omega T_{SW} = \pi$, where the expression is purely real – specifically, $e^{-j\pi} = \cos(\pi) = -1$, so the transfer function becomes

$$H_V(z)\Big|_{z=\frac{\omega_{SW}}{2}} = \frac{\alpha(-1)}{1-(1-\alpha)(-1)} = \frac{-\alpha}{2-\alpha} \quad (12)$$

The condition for stability therefore requires that $\alpha < 2$. The system is outside of the Region of Convergence (ROC) for $\alpha > 2$, while the system response is a sustained oscillation with $\alpha = 2$. It is intuitive from the time-domain expression in (3) that any condition for which the magnitude of $(1-\alpha)$ equals or exceeds 1.0, the state variable $i_v[n]$ will build rather than decay. Recall that α is a function of inductor current slopes as well as the slope compensation parameter, m_{cmp}. Expanding (4) into (12) and rearranging terms, the amount of slope compensation necessary for stability is found by ensuring the following inequality is satisfied,

$$m_{cmp} > \frac{m_d - m_c}{2} \quad (13)$$

D. Comparison to Conventional Approach

In $[ref]$ Middlebrook, Tan state the condition for stability in the peak current controller per following (with the exception that (14) translates notation to symbols consistent with the current text.).

$$D'_{min} = \frac{0.5}{1+\frac{m_{cmp}}{m_{mc}}} \quad (14)$$

For consistency with the inequality stated in (13), the quantity in (14) will be re-expressed as an inequality defining the values for D' for which the controller is stable,

$$D' > \frac{0.5}{1+\frac{m_{cmp}}{m_c}} \quad (15)$$

The steady-state condition within the peak current mode controller occurs when $i_v[n] - i_v[n-1]$. Evaluation of (1) in the steady state condition yields the following.

$$DT_sSWm_c - D'T_{SW}m_d = 0 \quad (16)$$

Substituting $D = (1 - D')$, the expression in (16) is manipulated into the following form.

$$D' = \frac{m_c}{m_c + m_d} \quad (17)$$

Combining (15) and (17),

$$\frac{m_c}{m_c + m_d} > \frac{0.5}{1+\frac{m_{cmp}}{m_c}} \quad (18)$$

Then solving (18) for slope compensation yields the following.

$$m_{cmp} > \frac{m_d - m_c}{2} \quad (19)$$

It is now apparent that (19) and (13) are in agreement.

E. Peak Current Controller magnitude response

In addition to evaluating peak current controller stability the expression in (12) may be rearranged to express a desired peak magnitude response in terms of the coefficient α.

$$\alpha = 2\frac{|H_v(z)|}{1+|H_v(z)|}\Big|_{z=\frac{1}{2}\omega_{SW}} \quad (20)$$

Expanding α from (4) and using additional algebraic manipulation, the amount of slope compensation corresponding to a pre-determined magnitude response is obtained.

$$m_{cmp} = \frac{1+|H_v(z)|}{2|H_v(z)|}(m_c + m_d) - m_c\Big|_{z=\frac{1}{2}\omega_{SW}} \quad (21)$$

Plotting a series of magnitude responses for values of α corresponding to a (notch) gain of -9 dB, increasing in 3 dB steps to +9 dB is shown below.
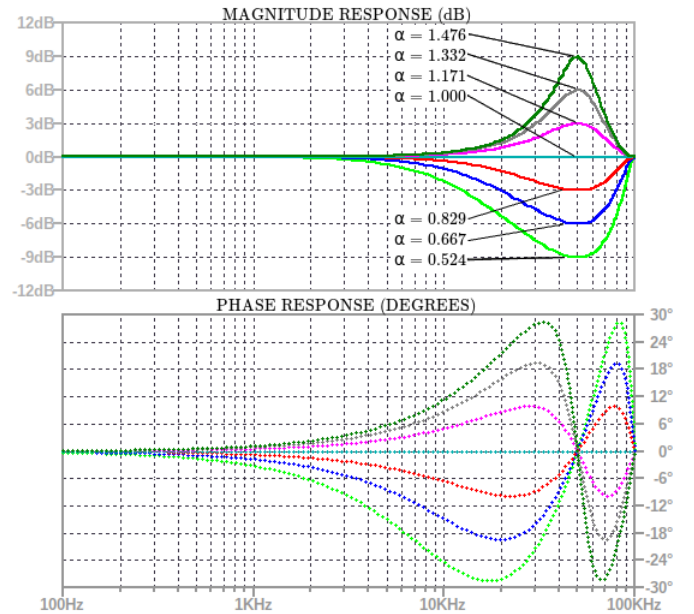

Fig. 4: Peak current controller frequency response, $H_v(z)$, plots with different values of α ($F_{SW} = 100kHz$).

The utility of having slope compensation expressed as a function of peak magnitude response is apparent when considering switched-mode converter design flow. For example, one can identify the minimum slope compensation required to achieve a desired amount of gain margin at $\frac{1}{2}F_{SW}$.

F. Reversing the Zero-Order-Hold Assumption

Derivation of the transfer function for valley currents assumes all values fed into the peak current mode controller were sampled at the rising edge of the switching clock and held for the entire period. Performing analysis under said assumption implicitly low-pass filters the input signal with a moving-average filter during the sampling process.

In the physical system, no such filtering is applied in the sampler, so the consequence of this operation must be reversed if the sampled system frequency response is to accurately describe the sampler as it actually behaves.

Because input voltages and inductor currents were sampled at the rising edge of the primary switching signal, these errors may all be simultaneously corrected by a single filtering operation applied to $\hat{i_v}[n]$.

The ZOH reversal filter is the frequency-domain inverse of the ZOH function. The ZOH frequency response is documented in [ref], and the inverse of this function stated below as H_{IZOH}, representing "Inverse Zero-Order-Hold".
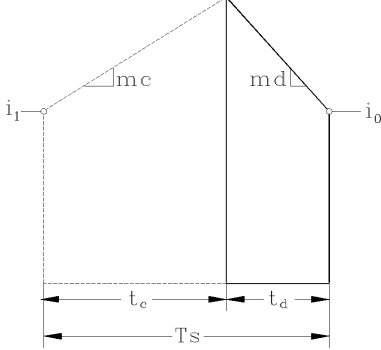
$$H_{IZOH}(s) = \frac{s}{1 - e^{-sT_{SW}}} \tag{22}$$

Fig. 5: Inductor current waveform illustrated as a geometric problem.

V. Cycle Average Current as FIR Filter

The inductor energy stored and released per switching cycle is a discrete quantity which may be expressed as a function of valley currents. If other quantities feeding into the waveform geometry are treated as sampled values (held constant over the switching interval), then the problem of relating average inductor currents to valley currents is reduced to that of a simple geometry problem as illustrated in Fig. 5. Since all quantities defining the inductor waveform begin and end within the same switching cycle, the valley-to-average-current transfer function response is finite and limited to a single switching cycle.

The set of parameters needed to express the area enclosed in the geometric shape illustrated in Fig. 5 are i_0, i_1, m_c, m_d, and T_{SW}. The anchor points identified as i_0 and i_1 serve as the interface linking the geometric problem to valley currents.

A noteworthy benefit of describing the discrete energy-per-cycle quantity as a function of valley current is that the system's core transfer function is agnostic to the control scheme implemented. For example, whether voltage mode, peak-current mode, quasi-resonant or even hysteretic control, the geometric problem presented in Fig. 5 remains unchanged.

Referring back to the equivalent circuit models presented in Fig. 1 it is apparent that the discharging and charging cycle currents must be treated as separate geometric problems if a generalized model is to be had from this approach.

A. Geometric Area of Charging Current

The average charging current is expressed as an integral of the geometric shape in Fig. 5 over the charging interval, $t = 0$ to $t = t_c$.

$$i_{cg} = \frac{1}{T_{SW}} \int_0^{t_c} (i_1 + m_c t) dt \tag{23}$$

The integral expressed in (23) evaluates to the following:

$$i_{cg} = \frac{t_c}{T_{SW}} i_1 + \frac{m_c t_c^2}{2 T_{SW}} \tag{24}$$

It is necessary to further expand (24) in terms of defined system constants and signals. To this end, the following equality is easily derived by inspection of Fig. 5.

$$m_c t_c + i_1 = m_d (T_{SW} - t_c) + i_0 \tag{25}$$

Where (25) is used to solve for the unknown, t_c, in terms of known quantities.

$$t_c = \frac{i_0 - i_1 + T_{SW} m_d}{m_c + m_d} \tag{26}$$

Substituting (26) into (24) the following solution for i_{cg} is obtained with sufficient use of algebraic simplification.

$$i_{cg} = a_{cg} i_0^2 + b_{cg} i_1^2 + c_{cg} i_0 i_1 + d_{cg} i_0 + e_{cg} i_1 + f_{cg} \tag{27}$$

Where the constants are expanded per below,

$$a_{cg} = \left(\frac{1}{2 T_{SW}} \right) \frac{m_c}{m_c^2 + 2 m_c m_d + m_d^2}$$

$$b_{cg} = - \left(\frac{1}{2 T_{SW}} \right) \frac{m_c + 2 m_d}{m_c^2 + 2 m_c m_d + m_d^2}$$

$$c_{cg} = \left(\frac{1}{T_{SW}} \right) \frac{m_d}{m_c^2 + 2 m_c m_d + m_d^2}$$

$$d_{cg} = \frac{m_c m_d}{m_c^2 + 2 m_c m_d + m_d^2}$$

$$e_{cg} = \frac{m_d^2}{m_c^2 + 2 m_c m_d + m_d^2}$$

$$f_{cg} = \left(\frac{T_{SW}}{2} \right) \frac{m_c m_d^2}{m_c^2 + 2 m_c m_d + m_d^2}$$

B. Geometric Area of Discharging Current

The process for finding a canonical solution for the discharging current follows the same process used for finding the average charging current. In this case the problem is simplified by reversing the shape in Fig. 5 and evaluating an integral having the same form as (23), substituting i_0, m_d and t_d for the initial current, slope and time variable.

$$i_{dg} = \frac{1}{T_{SW}} \int_0^{t_d} (i_0 + m_d t) dt \tag{28}$$

The integral in (28) evaluates to the following.

$$i_{dg} = \frac{t_d}{T_{SW}} i_0 + \frac{m_d t_d^2}{2 T_{SW}} \tag{29}$$

Using the identity $t_d = T_{SW} - t_c$, (29) becomes the following.

$$i_{dg} = \frac{T_{SW} - t_c}{T_{SW}} i_0 + \frac{m_d (T_{SW} - t_c)^2}{2 T_{SW}} \tag{30}$$

and then substituting (26) into (30), the solution for i_{dg} is seen to have the same form as (27), differing only by the set of coefficients characterizing the familiar polynomial expression.

$$i_{dg} = a_{dg} i_0^2 + b_{dg} i_1^2 + c_{dg} i_0 i_1 + d_{dg} i_0 + e_{dg} i_1 + f_{dg} \tag{31}$$

Where the constants are expanded per below.

$$a_{dg} = -\left(\frac{1}{2 T_{SW}}\right) \frac{2 m_c + m_d}{m_c^2 + 2 m_c m_d + m_d^2}$$

$$b_{dg} = \left(\frac{1}{2 T_{SW}}\right) \frac{m_d}{m_c^2 + 2 m_c m_d + m_d^2}$$

$$c_{dg} = \left(\frac{1}{T_{SW}}\right) \frac{m_c}{m_c^2 + 2 m_c m_d + m_d^2}$$

$$d_{dg} = \frac{m_c^2}{m_c^2 + 2 m_c m_d + m_d^2}$$

$$e_{dg} = \frac{m_c m_d}{m_c^2 + 2 m_c m_d + m_d^2}$$

$$f_{dg} = \left(\frac{T_{SW}}{2}\right) \frac{m_c^2 m_d}{m_c^2 + 2 m_c m_d + m_d^2}$$

C. Small-Signal Analysis of the Non-LTI Inductor Currents

It is no surprise (27) and (31) follow the same form since the geometric shapes are fundamentally similar. This commonality affords the convenience of having a generalized solution for the small signal model since the charging and discharging currents differ only in specific values used for the coefficients.

The formulae expressed in (27) and (31) constitute a pair of non-LTI FIR filters when the geometric shape represents inductor current, specifically,

$$i_0 = i_v[n]$$
$$i_1 = i_v[n-1] \tag{32}$$

This system can be understood as an LTI filter if the signals and response are constrained to infinitesimal amplitude, as though operating on a linear tangent at a point on the quadratic curve. This treatment of nonlinear systems is more commonly known as small-signal analysis, and treated in greater detail in [ref].

In this document discussion of small-signal analysis theory will be omitted, but the mechanics of this technique are introduced as a segue into the analysis. Considering the general form of a nonlinear function, $y = f(x)$, the function is approximated as linear at an operating point x_0. The approximation becomes increasingly accurate as deviations from x_0 are reduced in amplitude.

The linearized function is expressed using a partial derivative of $f(x)$ with respect to x,

$$G_{lin} = \left. \frac{\partial f(x)}{\partial x} \right|_{x=x_0} \tag{33}$$

Where G_{lin} is the equivalent linear gain on small deviations about x_0. In this case, x can be reinterpreted as,

$$y \approx f(x_0) + \Delta_x G_{lin} \tag{34}$$

where Δ_x represents a small perturbation superimposed on x when biased at operating point x_0. Since DC offsets within the transfer function are already captured in steady-state analysis, the small-signal transfer function is simplified to express only changes about the operating point, more specifically,

$$\Delta_y = \Delta_x G_{lin} \tag{35}$$

where Δ_y is the amount of change in y due to a small change in x with DC offsets absent from the expression; therefore, (35) is the small-signal transfer function for $y = f(x)$.

Now having briefly outlined the process, this will be applied to the generalized form of (27) and (31). Below the quantity i_{avg} is used as a placeholder for i_{cg} and i_{dg} to generalize the expression.

$$i_{avg} = a i_0^2 + b i_1^2 + c i_0 i_1 + d i_0 + e i_1 + f \tag{36}$$

In this case there are two independent variables, i_0 and i_1, so the partial derivative must be evaluated for both variables. One helpful observation is the preceding IIR filter stage is also presumed to be settled at steady state operating conditions, hence $i_v[n] = i_v[n-1] = i_{v\infty}$, where $i_{v\infty}$ is used to identify the final steady-state value for the valley current.

$$\Delta_{avg} = \Delta_0 \left. \frac{\partial i_{avg}}{\partial i_0} \right|_{i_1 = i_{v\infty}} + \Delta_1 \left. \frac{\partial i_{avg}}{\partial i_1} \right|_{i_0 = i_{v\infty}} \tag{37}$$

where,

$$\Delta_0 \text{ represents a small change in } i_0$$
$$\Delta_1 \text{ represents a small change in } i_1 \tag{38}$$

and the partial derivatives represent the small-signal gain on each input parameter.

Now let us consider the cycle-averaged output current to be the following,

$$i_{avg} \approx I_\infty + \Delta_{avg} \tag{39}$$

where I_∞ is the steady-state average current obtained given the condition that control input, $i_c[n]$, is held constant and

$i_v[n]$ is allowed to settle to its final steady state operating point as expressed in the following.

$$i_{v\infty} = \lim_{n\to\infty} i_v[n] = \lim_{n\to\infty} i_v[n-1] \quad (40)$$

Then i_{avg} from (36) is evaluated using (32) and (40),

$$I_\infty = i_{avg}\Big|_{\substack{i0=i_{v\infty}\\i1=i_{v\infty}}} = ai_{v\infty}^2 + bi_{v\infty}^2 + ci_{v\infty}i_{v\infty} + di_{v\infty} + ei_{v\infty} + f \quad (41)$$

which simplifies to the following after collecting like terms,

$$I_\infty = (a+b+c)i_{v\infty}^2 + (d+e)i_{v\infty} + f \quad (42)$$

Now having the DC operating point of the FIR filter, the gain on small perturbations about this operating point remains to be determined. For this, (36) is evaluated using terms defined in (38) as substituted into (37).

$$\Delta_{avg} = \frac{\partial}{\partial i_0}\left[ai_0^2 + bi_1^2 + ci_0i_1 + di_0 + ei_1 + f\right]\Delta_0\Big|_{i_0=i_{v\infty}}$$
$$+ \frac{\partial}{\partial i_1}\left[ai_0^2 + bi_1^2 + ci_0i_1 + di_0 + ei_1 + f\right]\Delta_1\Big|_{i_1=i_{v\infty}} \quad (43)$$

Evaluating (43) results in the following expression for small-signal changes in average currents.

$$\Delta_{avg} = \left(2ai_{v\infty} + ci_{v\infty} + d\right)\Delta_0 + \left(2bi_{v\infty} + ci_{v\infty} + e\right)\Delta_1 \quad (44)$$

In which the parenthetical expressions from (44) represent a set of coefficients which are further abstracted per the following.

$$k_0 = 2ai_{v\infty} + ci_{v\infty} + d$$
$$k_1 = 2bi_{v\infty} + ci_{v\infty} + e \quad (45)$$

Recall geometrically the quantity Δ_{avg} is a small change to the area bounded by the inductor current waveform during a single switching cycle as a function of small changes to the anchor points i_0 and i_1, expressed as Δ_0 and Δ_1. The geometry problem has been set up for re-interpretation using a symbolic convention consistent with more widely known literature.

$$\hat{i}_{avg} = k_0\hat{i}_v[n] + k_1\hat{i}_v[n-1] \quad (46)$$

Where the circumflex notation (e.g. $\hat{i}[n]$) represents the AC small-signal response of a nonlinear system. The proposed translation is executed by interpreting the Δ_{avg}, Δ_0, and Δ_1 as peak-to-peak limits on arbitrary AC waveforms $\hat{i}_{avg}$, $\hat{i}[n]$ and $\hat{i}[n-1]$, respectively. Interpreting the geometric problem as shown in (46) has a more easily identifiable form of a first-order FIR filter.

The form of the FIR filter expressed in (46) is expanded to an expression of the AC transfer function between valley currents and average output currents for both charging and discharging cycles by substituting coefficients identified in (27) and (31), specifically,

$$\hat{i}_{cg} = k_{0_{cg}}\hat{i}_v[n] + k_{1_{cg}}\hat{i}_v[n-1] \quad (47)$$

for the charging cycle current, and

$$\hat{i}_{dg} = k_{0_{dg}}\hat{i}_v[n] + k_{1_{dg}}\hat{i}_v[n-1] \quad (48)$$

represents the discharging cycle current.

D. Continuous Time Approximation of FIR Averaging Filter

A well-documented phenomenon of the switched inductor discharge current response (commonly associated with a buck/boost or flyback topology) is the right-half-plane-zero (RHPZ) that shows up in the loop response. The system evaluated according to the equivalent circuit models of Fig. 1 indicates the RHPZ exists in buck and forward converters but its response is swamped by the complementary left-half-plane zero characteristic of the charging cycle current.

To give intuitive context for the following derivation the FIR responses of (47) and (48) are plotted as discrete-time systems overlaid with the corrected response (inverse ZOH), and continuous time approximation (conventional RHPZ).
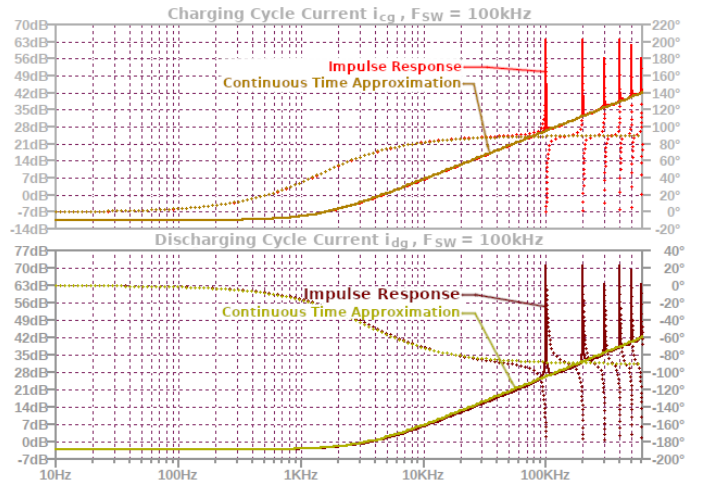

Fig. 6: Peak current controller transfer function of valley currents to charge/discharge currents (i_{cg}, i_{dg}) ($F_{SW} = 100kHz$).
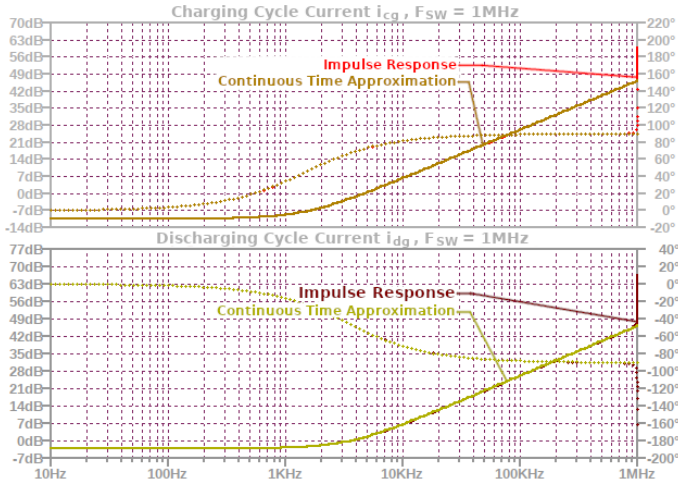
Fig. 7: Peak current controller transfer function of valley currents to charge/discharge currents (i_{cg}, i_{dg}) ($F_{SW} = 1MHz$).

1) Derivation of the RHPZ for Discharge Cycle Current:
From above plots it is apparent the impulse response based approach presented in this document traces the shape of the RHPZ as presented in conventional literature [ref]. It is here shown how the well-known RHPZ expression is readily obtained by evaluating (48) in the limit as $T_{SW} \to 0$.

First an intermediate variable is defined,

$$g_{dg} = \frac{1}{m_c^2 + 2m_c m_d + m_d^2} = \frac{1}{(m_c + m_d)^2} \quad (49)$$

which is a quantity common in every coefficient found in the discharging current polynomial expressed in (31). Now the small-signal FIR filter in (48) can be neatly expanded as follows.

$$\hat{i}_{dg}[n] = (2a_{dg} + c_{dg})i_{v\infty}\hat{i}_v[n] + d_{dg}\hat{i}_v[n]$$
$$+ (2b_{dg} + c_{dg})i_{v\infty}\hat{i}_v[n-1] + e_{dg}\hat{i}_v[n-1] \quad (50)$$

Then substituting a, b, c, d and e from coefficients of (31),

$$\frac{\hat{i}_{dg}[n]}{g_{dg}} = -\frac{m_c + m_d}{T_{SW}}i_{v\infty}\hat{i}_v[n] + m_c^2\hat{i}_v[n]$$
$$+ \frac{m_c + m_d}{T_{SW}}i_{v\infty}\hat{i}_v[n-1] + m_c m_d\hat{i}_v[n-1] \quad (51)$$

Re-expressing the difference equation in the continuous time domain with further rearrangement exposes a form of the derivative definition,

$$\frac{\hat{i}_{dg}(t)}{g_{dg}} = -\frac{\hat{i}_v(t) - \hat{i}_v(t - T_{SW})}{T_{SW}}(m_c + m_d)i_{v\infty}$$
$$+ m_c^2 i_{v\infty}\hat{i}_v(t) + m_c m_d i_{v\infty}\hat{i}_v(t - T_{SW}) \quad (52)$$

The expression in (52) exposes a differential equation if considering what happens when sampling frequency approaches infinity.

$$\lim_{T_{SW}\to 0} \frac{\hat{i}_{dg}(t)}{g_{dg}} = -(m_c + m_d)i_{v\infty}\frac{d}{dt}\hat{i}_v(t)$$
$$+ (m_c^2 + m_c m_d)i_{v\infty}\hat{i}_v(t) \quad (53)$$

The Laplace transform is then obtained by inspection (note the constant of integration is assumed zero since (54) represents the small-signal AC response),

$$\frac{\hat{I}_{dg}(s)}{g_{dg}} = -(m_c + m_d)i_{v\infty}\hat{I}_v(s)s + (m_c^2 + m_c m_d)i_{v\infty}\hat{I}_v(s) \quad (54)$$

Finally a transfer function is defined,

$$H_{dg}(s) = \frac{\hat{I}_{dg}(s)}{\hat{I}_v(s)} = g_{dg}(m_c + m_d)i_{v\infty}\left(\frac{m_c}{i_{v\infty}} - s\right)$$
$$= \frac{m_c + m_d}{(m_c + m_d)^2}i_{v\infty}\left(\frac{m_c}{i_{v\infty}} - s\right)$$
$$= \frac{i_{v\infty}}{m_c + m_d}\left(\frac{m_c}{i_{v\infty}} - s\right) \quad (55)$$

The conventional notion of a continuous time RHPZ is now apparent in (55). Further algebraic manipulation is required to demonstrate equivalence to a more commonly known form. The first item nonconformant to the conventional nomenclature is the steady-state valley current, $i_{v\infty}$, which must be re-expressed in terms of the steady-state i_{dg} if $R_{LOAD} = V_{dg}/i_{dg}$ is to be pulled out of this expression.

$$i_{dg} = \frac{L_m}{2V_{dg}T_{SW}}(i_{pk}^2 - i_{v\infty}^2) \quad (56)$$

where i_{pk} is the peak current, so the following substitution may be used.

$$i_{pk} = i_{v\infty} + \Delta_{IL} \quad (57)$$

The quantity Δ_{IL} is the steady-state ripple observed during CCM operation, further expanded to the following expression.

$$\Delta_{IL} = \frac{V_{cg}V_{dg}}{V_{cg} + V_{dg}}\frac{T_{SW}}{L_m} = D'\frac{V_{dg}T_{SW}}{L_m} \quad (58)$$

Substituting (58) and (57) into (56), the following is obtained.

$$i_{dg} = \frac{L_m}{2V_{dg}T_{SW}}\left(2\Delta_{IL}i_{v\infty} + \Delta_{IL}^2\right)$$
$$= \frac{L_m}{2V_{dg}T_{SW}}\left(2D'\frac{V_{dg}T_{SW}}{L_m}i_{v\infty} + \left(D'\frac{V_{dg}T_{SW}}{L_m}\right)^2\right)$$
$$= D'i_{v\infty} + D'^2\frac{V_{dg}T_{SW}}{2L_m} \quad (59)$$

Recall this system has been evaluated in the limit as $T_{SW} \to 0$, so the steady-state relationship between i_{dg} and $i_{v\infty}$ simplifies to the following.

$$i_{dg} = D'i_{v\infty} \tag{60}$$

Now, from (55) and (60) the location of the right-half-plane zero is extracted per following.

$$\omega_{RHPZ} = \frac{m_c}{i_{v\infty}} = \frac{V_{cg}}{L_m}\frac{D'}{i_{dg}} \tag{61}$$

Now ω_{RHPZ} is expressed using terms familiar within common literature, but further manipulation is needed for the equivalence to become obvious. Specifically, re-casting V_{cg} in terms of V_{dg}, where V_{dg} is equivalent to the output voltage in a flyback or buck-boost topology.

$$V_{cg} = V_{dg}\left(\frac{1}{D} - 1\right) \tag{62}$$

Then substituting (62) into (61) the following emerges.

$$\begin{aligned}
\omega_{RHPZ} &= \frac{V_{dg}}{i_{dg}L_m}D'\left(\frac{1}{D} - 1\right) \\
&= \frac{R_{LOAD}}{L_m}\left(\frac{D'}{D} - D'\right) \\
&= \frac{R_{LOAD}}{L_m D}D'(1 - D) \\
&= \frac{R_{LOAD}D'^2}{L_m D} \tag{63}
\end{aligned}$$

It is now apparent the expression in (63) agrees with the expression given in [2] for a buck-boost topology converter. The significance of the buck-boost output transfer function is due to dependence on the discharge cycle current such that $V_{OUT} = V_{dg}$ and $I_{OUT} = i_{dg}$, hence, $R_{LOAD} = \frac{V_{dg}}{i_{dg}}$.

The approach employed to arrive at this expression helps differentiate between sampling effects and the system dynamic response. Using the impulse response model shows this can be treated as a continuous-time system that obtains its input from a sampler. That is, sampling effects and system response have been decoupled.

2) Derivation of the LHPZ for the Charge Cycle Current: Derivation of the RHPZ was presented first because its relationship to the transfer function of a buck-boost topology is easily identifiable by comparison with prior work. The charging cycle current has a corollary response in the form of a Left-Half-Plane-Zero (LHPZ), but such is not typically expressed as an independent quantity within the conventional treatment of switched-mode converters. In topologies where charging cycle currents flow directly to the converter output (such as buck, forward), the conventional treatment expresses the transfer function as a quantity dependent upon the sum of charging and discharging currents, hence the LHPZ does not appear in the transfer function. As shown later, there is a cancellation between the LHPZ and RHPZ when the two current sources are summed at the output.

This section will identify the LHPZ in conventional terms of D, D' and R_{LOAD} and the subsequent section will briefly

explore how these sum in a buck topology to produce the typical transfer function for a peak current mode controller.

Based upon FIR coefficients previously defined we see the following is true,

$$g_{cg} = g_{dg} = \frac{1}{(m_c + m_d)^2} \tag{64}$$

which is a quantity common in every coefficient found in the charging current polynomial expressed in (27). Now the small-signal FIR filter in (47) can be neatly expanded as follows.

$$\begin{aligned}
\hat{i}_{cg}[n] = &(2a_{cg} + c_{cg})i_{v\infty}\hat{i}_v[n] + d_{cg}\hat{i}_v[n] \\
&+ (2b_{cg} + c_{cg})i_{v\infty}\hat{i}_v[n-1] + e_{cg}\hat{i}_v[n-1] \tag{65}
\end{aligned}$$

Then substituting a, b, c, d and e from coefficients of (27),

$$\begin{aligned}
\frac{\hat{i}_{cg}[n]}{g_{cg}} = &\frac{m_c + m_d}{T_{SW}}i_{v\infty}\hat{i}_v[n] + m_c m_d\hat{i}_v[n] \\
&- \frac{m_c + m_d}{T_{SW}}i_{v\infty}\hat{i}_v[n-1] + m_d^2\hat{i}_v[n-1] \tag{66}
\end{aligned}$$

Re-expressing the difference equation in the continuous time domain with further rearrangement exposes a form of the derivative definition,

$$\begin{aligned}
\frac{\hat{i}_{cg}(t)}{g_{cg}} = &\frac{\hat{i}_v(t) - \hat{i}_v(t - T_{SW})}{T_{SW}}(m_c + m_d)i_{v\infty} \\
&+ m_c m_d\hat{i}_v(t) + m_d^2\hat{i}_v(t - T_{SW}) \tag{67}
\end{aligned}$$

The expression in (67) exposes a differential equation if considering what happens when sampling frequency approaches infinity.

$$\begin{aligned}
\lim_{T_{SW}\to 0}\frac{\hat{i}_{cg}(t)}{g_{cg}} = &(m_c + m_d)i_{v\infty}\frac{d}{dt}\hat{i}_v(t) \\
&+ m_d(m_c + m_d)i_{v\infty}\hat{i}_v(t) \tag{68}
\end{aligned}$$

The Laplace transform is then obtained by inspection (note the constant of integration is assumed zero since (69) represents the small-signal AC response),

$$\frac{\hat{I}_{cg}(s)}{g_{cg}} = (m_c + m_d)i_{v\infty}\hat{I}_v(s)s + m_d(m_c + m_d)i_{v\infty}\hat{I}_v(s) \tag{69}$$

Finally a transfer function is defined,

$$\begin{aligned}
H_{cg}(s) = \frac{\hat{I}_{cg}(s)}{\hat{I}_v(s)} &= g_{cg}(m_c + m_d)i_{v\infty}\left(\frac{m_d}{i_{v\infty}} + s\right) \\
&= \frac{m_c + m_d}{(m_c + m_d)^2}i_{v\infty}\left(\frac{m_d}{i_{v\infty}} + s\right) \\
&= \frac{i_{v\infty}}{m_c + m_d}\left(\frac{m_d}{i_{v\infty}} + s\right) \tag{70}
\end{aligned}$$

The notion of a continuous time LHPZ is now apparent in (70). The following process is nearly identical to that outlined

in the prior section with specifics changed to frame this in relationship to properties of the charging cycle current.

$$i_{cg} = \frac{L_m}{2V_{cg}T_{SW}}(i_{pk}^2 - i_{v\infty}^2) \tag{71}$$

where i_{pk} is the peak current, so the following substitution may be used.

$$i_{pk} = i_{v\infty} + \Delta_{IL} \tag{72}$$

The quantity Δ_{IL} is the steady-state ripple observed during CCM operation, further expanded to the following expression.

$$\Delta_{IL} = \frac{V_{cg}V_{dg}}{V_{cg} + V_{dg}}\frac{T_{SW}}{L_m} = D\frac{V_{cg}T_{SW}}{L_m} \tag{73}$$

Substituting (73) and (72) into (71), the following is obtained.

$$\begin{aligned}
i_{cg} &= \frac{L_m}{2V_{cg}T_{SW}}\left(2\Delta_{IL}i_{v\infty} + \Delta_{IL}^2\right) \\
&= \frac{L_m}{2V_{cg}T_{SW}}\left(2D\frac{V_{cg}T_{SW}}{L_m}i_{v\infty} + \left(D\frac{V_{cg}T_{SW}}{L_m}\right)^2\right) \\
&= Di_{v\infty} + D^2\frac{V_{cg}T_{SW}}{2L_m} \tag{74}
\end{aligned}$$

Recall this system has been evaluated in the limit as $T_{SW} \to 0$, so the steady-state relationship between i_{cg} and $i_{v\infty}$ simplifies to the following.

$$i_{cg} = Di_{v\infty} \tag{75}$$

Now, from (70) and (75) the location of the left-half-plane zero is extracted per following.

$$\omega_{LHPZ} = \frac{m_d}{i_{v\infty}} = \frac{V_{dg}}{L_m}\frac{D}{i_{cg}} \tag{76}$$

Now ω_{LHPZ} is further distilled following the process used for ω_{RHPZ}. Specifically, re-casting V_{cg} in terms of V_{dg}, where V_{dg} is equivalent to the output voltage in a flyback or buck-boost topology.

$$V_{dg} = \frac{DV_{cg}}{D'} \tag{77}$$

Then substituting (77) into (76) the following emerges.

$$\begin{aligned}
\omega_{LHPZ} &= \frac{V_{cg}}{i_{cg}L_m}D\left(\frac{D}{D'}\right) \\
&= \frac{V_{cg}D^2}{i_{cg}L_mD'} \\
&= \frac{R_{IN}D^2}{L_mD'} \tag{78}
\end{aligned}$$

Since the quantity R_{IN} does not have an intuitive connection to the converter loading conditions, it is more meaningful to relate the LHPZ to the output loading condition, R_{LOAD}.

Backing up to (76), and using (75) the following form of the expression is obtained.

$$\omega_{LHPZ} = \frac{m_d}{i_{v\infty}} = \frac{V_{dg}D'}{i_{dg}L_m} = \frac{R_{LOAD}D'}{L_m} \tag{79}$$

The significance of (78) is the complementary form to the RHPZ, that is the D and D' terms are swapped, the load is reflected to the converter input, while the zero appears in left-half-plane. The expression in (79) relates the LHPZ location to R_{LOAD}, which is a more intuitive quantity.

3) Effect of Summing Charging and Discharging Currents: In some topologies such as the buck converter, the charging cycle current is summed with the discharging cycle current at the output. It will be shown the LHPZ and RHPZ cancel and do not have an effect on the composite output response.

First it will be convenient to express the complete transfer functions in further developed terms so the relationship to the conventional response is apparent.

$$\begin{aligned}
H_{cg}(s) &= \frac{i_{v\infty}}{m_c + m_d}\left(\frac{m_d}{i_{v\infty}} + s\right) \\
&= \frac{L_m i_{dg}}{D'(V_{cg} + V_{dg})}\left(\frac{R_{LOAD}D'}{L_m} + s\right) \\
&= \frac{i_{dg}L_mD}{V_{dg}D'}\left(\frac{R_{LOAD}D'}{L_m} + s\right) \\
&= \frac{L_mD}{R_{LOAD}D'}\left(\frac{R_{LOAD}D'}{L_m} + s\right) \tag{80}
\end{aligned}$$

Only the zero location and sign changes for discharging current, so below simplification steps are brief following on from (80).

$$\begin{aligned}
H_{dg}(s) &= \frac{i_{v\infty}}{m_c + m_d}\left(\frac{m_c}{i_{v\infty}} - s\right) \\
&= \frac{L_mD}{R_{LOAD}D'}\left(\frac{R_{LOAD}D'^2}{L_mD} - s\right) \tag{81}
\end{aligned}$$

The valley-to-output-current transfer function for a buck converter then becomes the following.

$$\begin{aligned}
H_{ibuck}(s) &= \frac{\hat{i}_{dg}(s) + \hat{i}_{cg}(s)}{\hat{i}_v(s)} = \frac{\hat{i}_{out}(s)}{\hat{i}_v(s)} \\
&= \frac{L_mD}{R_{LOAD}D'}\left(\frac{R_{LOAD}D'}{L_m} + s\right) \\
&\quad + \frac{L_mD}{R_{LOAD}D'}\left(\frac{R_{LOAD}D'^2}{L_mD} - s\right) \\
&= \frac{L_mD}{R_{LOAD}D'}\left(\frac{R_{LOAD}D'}{L_m} + s + \frac{R_{LOAD}D'^2}{L_mD} - s\right) \\
&= D + D' \\
&= D + 1 - D \\
&= 1 \tag{82}
\end{aligned}$$

The result demonstrated in (82) is intuitive given the inductor current geometry when charging and discharging cycles are combined into a single output. The main piece missing to

relate this to [ref Table 12.3, pg 470, Erickson] simple model is AC response of the peak current controller. For matching the simple model, the quantity (10) may be considered equal to its DC gain,

$$\frac{\hat{i}_v(s)}{\hat{i}_c(s)} \approx H_v(e^{j\omega})\Big|_{\omega=0} = \frac{\alpha e^{-j0}}{1-(1-\alpha)e^{-j0}}$$
$$= \frac{\alpha}{1-(1-\alpha)}$$
$$= 1 \tag{83}$$

In the simple model referenced, control-to-output is expressed as output voltage as a response to control current. The model assumes the output is a simple $R\|C$ network. In the equivalent circuit for a buck converter shown in Fig. 1 it can be seen the impulse response model for the output is then a current source in parallel with the RC network, hence,

$$\hat{v} = (\hat{i}_{cg} + \hat{i}_{dg})\frac{R}{1+sRC}$$
$$= \hat{i}_{out}\frac{R}{1+sRC} \tag{84}$$

where $R = R_{LOAD}$ and C is the output filter capacitor. From (82) and (83) it is apparent that $\hat{i}_{out} = \hat{i}_c$ if the current mode controller high frequency peaking effect is neglected. Using the stated assumptions the following is equivalent to (84),

$$\hat{v} = \hat{i}_c \frac{R}{1+sRC} \tag{85}$$

and finally the expression matching [ref Erickson] is obtained.

$$\frac{\hat{v}}{\hat{i}_c} = \frac{R}{1+sRC} \tag{86}$$

It will be asserted the more accurate model presented by Erickson would be reproduced by evaluating the impulse response for the output voltage to valley current transfer function, from which an equivalent small-signal output impedance could be expressed. The proposed exercise is not documented here.

E. Discrete to Continuous Reconstruction

The steady-state inductor current pulse shape includes information about the high-frequency response and (more importantly) the filter group delay. The sampled system derived to this point accurately reconstructs the system magnitude response up to half the Nyquist frequency, but fails to predict phase response in the band where gain margin might be evaluated. In this section it is shown how the sampled system is reconstructed when assuming small-signal perturbation.

The steady-state inductor current pulse may be considered analogous to a digital-to-analog converter's (DAC) reconstruction filter. A simple form of such a filter is the Zero-Order-Hold system, intuitively understood as latching and holding the sampled value in the DAC output until the next sampling interval is clocked. In the frequency domain the ZOH system is evaluated as a moving average filter that operates over the sampling interval. The Laplace transform of a single rectangular pulse constitutes the frequency domain transfer function of said filter.

In the context of the approach being developed in this document, the inductor current pulse shapes during the charging and discharging cycles are not square pulses as assumed by a ZOH function and such would here misrepresent the system frequency response. The geometry of the output pulse is known and the discrete-to-continuous reconstruction filters can be derived by a similar process used to characterize the frequency response of a ZOH DAC.

The FIR filters characterized by (47) and (48) define the discrete-time pulse train, representing a sampled version of average inductor currents. Using these samples to trigger pulses with shapes illustrated in Fig. 5, the transfer function is obtained for reconstructing the sampled system to its continuous time representation.

1) Frequency Response of Charging Current: Referring back to Fig. 5, the frequency response for the system reconstructing the charging-cycle currents is obtained by the following.

$$i_{cg} = \int_0^{t_c}(i_{v\infty}+m_c t)e^{-st}dt$$
$$= i_{v\infty}\left[\frac{-e^{-st}}{s}\right]_0^{t_c} + m_c\left[\left(\frac{-t}{s}-\frac{1}{s^2}\right)e^{-st}\right]_0^{t_c}$$
$$= i_{v\infty}\left(\frac{1-e^{-t_c}}{s}\right) + m_c\left(\frac{1-(1+st_c)e^{-st_c}}{s^2}\right) \tag{87}$$

2) Frequency Response of Discharging Current: Referring back to Fig. 5, the frequency response for the system reconstructing the discharging-cycle currents is obtained by the Laplace transform of the discharging current pulse. The process is similar to what was done in (87), so the intermediate step is omitted.

$$i_{dg} = \int_{t_c}^{T_{SW}+t_d}(i_{v\infty}+m_d t_d - m_d t)e^{-st}dt$$
$$= (i_{v\infty}+m_d t_d)\left(\frac{1-e^{-t_d}}{s}\right)e^{-st_c}$$
$$- m_d\left(\frac{1-(1+st_d)e^{-st_d}}{s^2}\right)e^{-st_c} \tag{88}$$

VI. Conclusion

Example inline citation [1], is a citation.

References

[1] Reference 1.
[2] Erickson, Maksimovic, Fundamentals of Power Electronics, 2nd Ed, transfer function salient characteristics, pg. 300, Table 8.2, Buck-Boost RHPZ.